

CHANGING FACE OF THE EXTRASOLAR GIANT PLANET, HD 209458 b

JAMES Y-K. CHO,^{1,5} KRISTEN MENU,^{2,6,7} BRADLEY M. S. HANSEN^{2,3,8} & SARA SEAGER^{4,5}

Draft version November 16, 2018

ABSTRACT

High-resolution atmospheric flow simulations of the tidally-locked extrasolar giant planet, HD 209458 b, show large-scale spatio-temporal variability. This is in contrast to the simple, permanent day/night (i.e., hot/cold) picture. The planet’s global circulation is characterized by a polar vortex in motion around each pole and a banded structure corresponding to ~ 3 broad zonal (east-west) jets. For very strong jets, the circulation-induced temperature difference between moving hot and cold regions can reach up to ~ 1000 K, suggesting that atmospheric variability could be observed in the planet’s spectral and photometric signatures.

subject headings: planetary systems – planets and satellites: general – stars: atmospheres – turbulence

1. INTRODUCTION

Roughly 100 gaseous giant planets are currently known to orbit nearby sun-like stars⁹. Many of those planets are located at very small orbital distances from their parent stars, where tidal forces are thought to maintain a rotation rate synchronous with the orbit—thus producing permanent day and night sides on the planet. This situation presents a new régime of atmospheric circulation, not encountered in our solar system: slowly-rotating giant planets, which are continuously exposed to intense stellar heating on the same side. Measuring the resulting temperature structure on these planets is a major goal of current and future observational programs. In this *Letter*, we report on high-resolution, fully-turbulent global simulations of the atmospheric flow on HD 209458 b, presently the only close-in extrasolar giant planet (CEGP) with a measured mass (M_p) and radius (R_p).

The parent star of HD 209458 b shows discernible brightness decrements every 3.5 days, due to occultations by the planet as it transits across the star. This property has recently led to precise measurements of M_p and R_p (Charbonneau et al. 2000; Henry et al. 2000; Mazeh et al. 2000), confirming its giant nature. It has also allowed the detection of sodium absorption, providing the first probe of the planet’s atmosphere (Charbonneau et al. 2002). According to the standard planetary formation picture, HD 209458 b is expected to have formed at a large distance (> 1 AU) from its parent star (see, e.g., Boss 1996) and migrated inward (Goldreich & Tremaine 1980; Lin et al. 1996; Murray et al. 1998), quickly ($\lesssim 10$ Myr) reaching its present distance of only 0.046 AU from the star (see

e.g., Burrows et al. 2000). There, it was forced by tidal effects to permanently present the same face to its star (see, e.g., Goldreich & Soter 1966)—as the Moon does to the Earth. From this synchronization, the rotation period of the CEGP is known (same as its orbital period of 3.5 days). However, unlike our Moon with its insignificant atmosphere, HD 209458 b is expected to possess vigorous meteorology and associated horizontal transport of heat and chemical species, due to the presence of a thin, stable (radiative) atmospheric region above the convective interior (Guillot et al. 1996; Seager & Sasselo 1998).

2. MODEL

We model the stable region of HD 209458 b’s atmosphere as a shallow layer of hydrostatically balanced, frictionless gas—moving under the influence of gravitational and Coriolis accelerations. The motion of such a layer enveloping a planet is governed by the equivalent barotropic formulation of the shallow-water equations on a rotating sphere (Salby 1989):

$$\frac{\partial \mathbf{v}}{\partial t} + \mathbf{v} \cdot \nabla \mathbf{v} = -g \nabla h - f \mathbf{k} \times \mathbf{v} + \mathcal{F}_a, \quad (1)$$

$$\frac{\partial h}{\partial t} + \mathbf{v} \cdot \nabla h = -K h \nabla \cdot \mathbf{v} + \mathcal{F}_d, \quad (2)$$

where $\mathbf{v} = \mathbf{v}(\lambda, \varphi, t)$ is the horizontal velocity with λ and φ the longitude and latitude, respectively; $h = h(\lambda, \varphi, t)$ is the thickness of the modeled layer, proportional to the temperature; $f = 2\Omega \sin \varphi$ is the Coriolis parameter, where Ω is the rotation rate of the planet; \mathbf{k} is the local unit vector normal to the planetary surface; g is the gravitational

¹Spectral Sciences Inc., 99 South Bedford Street, #7, Burlington, MA 01803, USA

²Princeton University, Department of Astrophysical Sciences, Princeton, NJ 08540, USA

³Division of Astronomy, UCLA, 8971 Math Sciences, Los Angeles, CA 90095, USA

⁴School of Natural Sciences, Institute for Advanced Study, 1 Einstein Drive, Princeton, NJ 08540, USA

⁵Present address: Carnegie Institution of Washington, Department of Terrestrial Magnetism, 5241 Broad Branch Rd. NW, Washington, DC 20015, USA

⁶Chandra Fellow

⁷Present address: Department of Astronomy, P.O. Box 3818, University of Virginia, Charlottesville, VA 22903, USA

⁸Hubble Fellow

⁹see, e.g., <http://www.obspm.fr/encycl/encycl.html> and <http://exoplanets.org/almanacframe.html>

acceleration; $\mathcal{F}_a = -g\nabla\eta(1 - \exp\{-t/\tau_a\})\cos(\varphi)\cos(\lambda)$ and $\mathcal{F}_d = -(h - h_E)/\tau_d$ are, respectively, the adiabatic and diabatic thermal forcing, representing uneven hemispheric heating and cooling due to synchronization; τ_a and τ_d are characteristic e -folding times; $h_E = H + \eta\cos(\varphi)\cos(\lambda)$ is the equilibrium thickness; η , and H are constants; and, $\mathcal{K} = R/c_p$, where R is the specific gas constant and c_p is the specific heat at constant pressure.

The nonlinear equations (1) and (2) describe circulations in which the motion field is vertically aligned over one or more pressure scale heights, H_p . They are column-integrated representation of the equations used in general circulation models and are solved numerically using the highly-accurate pseudospectral algorithm (Eliassen, Mechenhauer & Rasmussen 1970; Orszag 1970). Approximately 150 simulation runs with up to T341 (1024×512 grid) resolution have been performed to explore the full physical and numerical parameter-space available for the HD 209458 b atmosphere. The details of the full exploration are described elsewhere (Cho et al. 2003). Here, we emphasize only the main robust features from the large number of simulations—namely, the emergence of long timescale variability due to moving polar vortices and “thermal” spots of high contrast from the background temperature field.

High-resolution, shallow-layer barotropic models in spherical geometry have been successfully used to model the atmospheric dynamics of the solar system gaseous giant planets (Williams 1978; Cho & Polvani 1996a), as well as stratospheric (stable region) phenomena on the Earth (see, e.g., Jukes & McIntyre 1987). An alternate model of observed cloud level circulation on Jupiter as a surface expression of deep convective columns, oriented parallel to the planetary rotation axis, also exists (Sun et al. 1993; Schubert & Zhang 2000). However, only the shallow-layer model has thus far qualitatively reproduced the essential features (bands, zonal winds, persistent spots, and anticyclonic dominance) on all of the giant planets in our solar system using only the observed values of physical parameters (Cho & Polvani 1996a).

For HD 209458 b, we adopt parameter values where known (Charbonneau et al. 2000; Henry et al. 2000; Mazeh et al. 2000): $\mathcal{K} = 0.29$, $g = 8 \text{ m s}^{-2}$, $R_p = 10^8 \text{ m}$, $\Omega = 2.1 \times 10^{-5} \text{ s}^{-1}$, and $H = 2 \times 10^6 \text{ m}$. The last ($= H_p/\mathcal{K}$) represents the global mean layer thickness, whose value corresponds to the equivalent blackbody temperature ($T_{\text{atm}} \approx 1400 \text{ K}$ for a Bond albedo, $A = 0.2$; the results presented here, however, are insensitive to the precise choice of T_{atm} and A). The values for two required parameters— η , the amplitude of hemispheric thermal forcing, and U , the characteristic wind speed related to the global mean kinetic energy—are not known and hence varied. From run to run, η is varied from 0 to $0.4H$, corresponding respectively to no heating and maximum substellar-point heating in the absence of atmospheric motion; U is varied from 50 m s^{-1} to 1000 m s^{-1} , roughly the observed value for Jupiter (Ingersoll 1990) and the value expected from a simple thermal wind balance (Showman & Guillot 2002), respectively. Note that the latter value leads to a nonlinearly-balanced wind field which can locally approach the sound speed ($\sim 2700 \text{ m s}^{-1}$); on all observed atmospheres in our solar system, U does not exceed $\sim 400 \text{ m s}^{-1}$ (Beatty & Chaiken 1990). We have carefully

studied the effects of U on the variability and thermal contrast and find that, while a variability in the flow is a generic feature for HD 209458 b, a significant thermal contrast generally requires a small η or a large U . In the following, we give an example of the expected generic flow pattern and then describe a typical flow-induced thermal variability which may be observationally relevant.

3. RESULTS

Fig. 1 shows an instantaneous atmospheric flow field on HD 209458 b at dynamic equilibrium from one of our simulations with $U = 400 \text{ m s}^{-1}$ and η corresponding to a maximum day/night temperature difference of 180 K. The flow exhibits considerable complexity and variability: it is characterized by a broad equatorial band containing thin, undulating filamentary structures at low and middle latitudes and displaced, translating circumpolar vortices at the rotation poles. The large undulations at low latitudes, which can roll up into small vortices, are due to high-amplitude Rossby (planetary) waves. In addition to being responsible for weather, the planetary waves efficiently stir and mix tracers (e.g., clouds, chemical species, potential vorticity) when they break, homogenizing the region in which the breakings occur (Jukes & McIntyre 1987). In contrast, polar vortices sequester air inside, their sharp boundaries serving as robust barriers to material transport between their interiors and the well-mixed interstitial regions. The overall flow is similar to that of Earth’s winter stratosphere.

The complex flow of Fig. 1 corresponds to a global circulation pattern of 3 zonal jets, shown in Fig. 2. Jets are atmospheric flow structures, which are obtained by longitudinally averaging the eastward wind at each latitude. The pattern in Fig. 2 naturally evolves from an initially random flow without jets, with the basic profile forming approximately at day 20. The emergence of jets from a random field is a generic feature of turbulent flows in a differentially rotating shallow layer (Rhines 1975; Williams 1978; Cho & Polvani 1996b). For the extreme values of U considered with all other parameters held fixed, 2 or 4 jets are also possible. However, once formed, the jets do not change qualitatively—even under applied thermal forcing—for up to several hundred HD 209458 b days, the duration of the simulation.

The presence of a low number of broad jets, along with polar vortices, leads to a circulation pattern which is markedly different from that of cloud-top Jupiter. Although CEGPs are sometimes dubbed “hot Jupiters”, the circulation pattern is more like that of Uranus or Neptune, or even Earth, than that of Jupiter or Saturn, which have ~ 10 narrow jets (Ingersoll 1990). Dynamically, this is expected given roughly the factors of ten greater T_{atm} and ten slower rotation rate of HD 209458 b compared to Jupiter. The combined effect, giving the flows in Figs. 1 and 2, is characterized by the Rossby deformation scale, $L_D = (\mathcal{K}gH)^{1/2}/f$, which is to be compared with R_p . Generally, $L_D/R_p \ll 1$ is required for a Jupiter-like multiple-jet circulation pattern without pronounced polar vortices at the cloud-top. For HD 209458 b, $L_D/R_p \sim 1$.

Jets and vortices/eddies can strongly influence the overall thermal structure by transporting heat. Since the state of the HD 209458 b’s cloud-top is not likely to be at rest and driven solely by stellar heating, we delay the applica-

tion of thermal forcing (in contrast to Showman & Guillot 2002) until the flow field self-organizes into the pattern in Fig. 2. Dynamically, this is a likely flow state of HD 209458 b in the presence of weak or uniform heating (i.e., at *pre-synchronization*). The forcing is slowly increased to the specified value of η over a characteristic radiative equilibrium time, $\tau_r = 10$ days, appropriate for ~ 1 bar pressure level on HD 209458 b. At this depth, $\tau_r \gg \tau_c$ (where $\tau_c = R_p/U$ is the characteristic circulation time), signifying a large distance advection of air mass before it warms or cools appreciably. The results presented here do not change qualitatively with the value of τ_r (~ 0 –100 days), using either an adiabatic ($\mathcal{F}_a, \tau_a = \tau_r$) or a diabatic ($\mathcal{F}_d, \tau_d = \tau_r$) representation of thermal forcing.

At each point on the planet, the layer thickness is related to the temperature field, $T(\lambda, \varphi, t) = hg/c_p$, via the hypsometric relation (Holton 1992; Salby 1989). In our simulations with small η or large U , the T field exhibits a generic feature which is in direct contrast to the simple permanent day/night picture. Fig. 3 shows the T distribution (from the same run of Figs. 1 and 2) at several different times. Note that the warmest and the coldest regions are not located at the sub-stellar and the anti-stellar “thermal poles” (at the equator), respectively. Instead, the temperature extrema are located near the rotation poles, inside a coherent hot/cold spot pair at each pole. Nor are the extrema stationary: they revolve around the poles with a period of ~ 25 days in this case. The movement leads to a distribution that for a time has the temperature minimum actually on the “hot” day side and the maximum on the “cold” night side. In addition, the temperature difference between the two extrema is large and strongly asymmetric; here, the difference is ~ 300 K, with the diffuse hot region ~ 70 K above and the sharp cold region ~ 230 K below T_{atm} . For the case with $U = 1000 \text{ m s}^{-1}$, the difference reaches ~ 1000 K, with a temperature minimum of ~ 800 K below T_{atm} at the core of the cold spots.

4. DISCUSSION

The presence of high-contrast hot and cold spots on HD 209458 b induces spatio-temporal variability, which may produce detectable fluctuations in observational signatures. Sensitive enough infrared flux measurements (e.g., such as those possible with SIRTf) could reveal variability in time during an orbit of the planet as different faces are seen from Earth, as well as from orbit to orbit as

the spots (polar vortices) revolve about the rotation poles. The lack of detectable variability would thus point toward either an obscuring uniform haze overlying the modeled region or an inefficient conversion of stellar irradiation to atmospheric kinetic energy. In the latter case, the formed spots are weak (i.e., small temperature/thickness perturbation) and thermal forcing which produces bulging in the modeled layer of more than several percent overwhelms any temperature variability due to atmospheric motion. The equilibrium day/night temperature is then robustly maintained.

The extreme conditions inside the spots in our calculations suggest several additional potential observables since absorption levels, albedo, intrinsic thermal emission, and presence, type, or height of clouds could all be different within the different spots. The spatially integrated spectrum, therefore, can be different from the uniform planet case. For example, enhanced levels of CH_4/CO abundance inside the cold spots are possible, given the value of T_{atm} used (Seager et al. 2000). Similarly, condensates, such as MgSiO_3 (enstatite), may also be found inside the diffuse hot spots, where temperatures may be high enough (Sudarsky et al. 2000; Seager et al. 2000). If the temperature at radiative equilibrium is actually higher than assumed (e.g., ~ 2000 K), the opposite situation may occur— MgSiO_3 may be found in the cold spots. In addition, by sequestering chemically active species and periodically exposing them to the stellar irradiation (as the spots revolve around the poles), the spots could also affect atomic number densities and could be part of the explanation for the recently observed low abundance of Na I on HD 209458 b (Charbonneau et al. 2002).

ACKNOWLEDGMENTS

J.Y.-K.C. acknowledges the hospitality of the Institute for Advanced Study, where the initial part of this work was completed, and R. Levine for helpful discussions. K.M. is supported by NASA under Chandra Fellowship grant PF9-10006, awarded by the Smithsonian Astrophysical Observatory for NASA under contract NAS8-39073. B.M.S.H. is supported by the Hubble Fellowship grant HF-01120.01-99A, awarded by the Space Telescope Science Institute, which is operated by the Association of Universities for Research in Astronomy, Inc. for NASA under contract NAS 5-26555. S.S. is supported by the W.M. Keck foundation. We thank the referee, W. Hubbard, for comments.

REFERENCES

- Beatty, J.K. & Chaiken, J. 1990, *The New Solar System* (Sky Publishing Corp. and Cambridge Univ. Press: Cambridge, MA) 3rd ed.
 Boss, A.P. 1996, *ApJ*, 469, 906
 Burrows, A. et al. 2000, *ApJ*, 534, L97
 Charbonneau, D., Brown, T.M., Latham, D.W. & Mayor, M. 2000, *ApJ*, 529, L45
 Charbonneau, D., Brown, T.M., Noyes, R.W. & Gilliland, R.L. 2002, *ApJ*, 568, 377
 Cho, J.Y.-K., Menou, K., Hansen, B.M.S., & Seager, S. 2003, in preparation.
 Cho, J.Y.-K. & Polvani, L.M. 1996a, *Science*, 273, 335
 Cho, J.Y.-K. & Polvani, L.M. 1996b, *Phys. Fluids*, 8, 1531
 Eliassen, E., Mechenhauer, B. & Rasmussen, E. 1970, Technical Report No. 2, Institut for Teoretisk Meteorologi, Kobenhavns Universitet, Denmark
 Goldreich, P. & Soter, S. 1966, *Icarus*, 5, 375
 Goldreich, P., & Tremaine, S. 1980, *ApJ*, 241, 425
 Guillot, T., Burrows, A., Hubbard, W.B., Lunine, J.I. & Saumon, D., 1996, *ApJ*, 459, L35
 Henry, G., Marcy, G.W., Butler, R.P. & Vogt, S.S. 2000, *ApJ*, 529, L41
 Holton, J.R. 1992, *Introduction to Dynamic Meteorology* (Academic Press: San Diego)
 Ingersoll, A.P. 1990, *Science*, 248, 308
 Jukes, M.N. & McIntyre, M.E. 1987, *Nature*, 328, 590
 Lin, D.N.C., Bodenheimer, P. & Richardson, D.C. 1996, *Nature*, 380, 606
 Mazeh, T. et al. 2000, *ApJ*, 532, L55
 Murray, N., Hansen, B., Holman, M. & Tremaine, S. 1998, *Science*, 279, 69
 Orszag, A. 1970, *J. Atmos. Sci.*, 27, 890
 Rhines, P.B. 1975, *J. Fluid Mech.*, 69, 417
 Salby, M.L. 1989, *Tellus*, 41A, 48
 Schubert, G. & Zhang, K. 2000, in *ASP Conf. Ser.* 212, From Giant Planets to Cool Stars, ed. C.A. Griffith & M.S. Marley (San Francisco: ASP), 210

- Seager, S. & Sasselov, D.D. 1998, ApJ, 502, L157
Seager, S., Whitney, B.A. & Sasselov, D.D. 2000, ApJ, 540, 504
Showman, A.P. & Guillot, T. 2002, A&A, 385, 166
Sudarsky, D., Burrows, A & Pinto, A.A. 2000, ApJ, 538, 885
Sun, Z.-P., Schubert, G. & Glatzmeier, G.A. 1993, Science, 260, 661
Williams, G.P. 1978, J. Atmos. Sci., 35, 1399

FIG. 1.— Two views of the dynamical flow tracer, potential vorticity (Holton 1992), at day (=year) 55 from our T341 (1024×512 grid resolution) simulation of the atmospheric circulation of HD 209458 b: a) orthographic projection centered at the anti-stellar point (AS) on the night side and b) polar-stereographic projection centered at the north pole (NP). 1 PVU = $4 \times 10^{-27} \text{ s}^{-1} \text{ m}^1/\text{K}$. The global flow is characterized by two circumpolar cyclonic (rotating in the same direction as the planet—counter-clockwise in the figure) vortices at high latitudes and high-amplitude planetary waves at low latitudes.

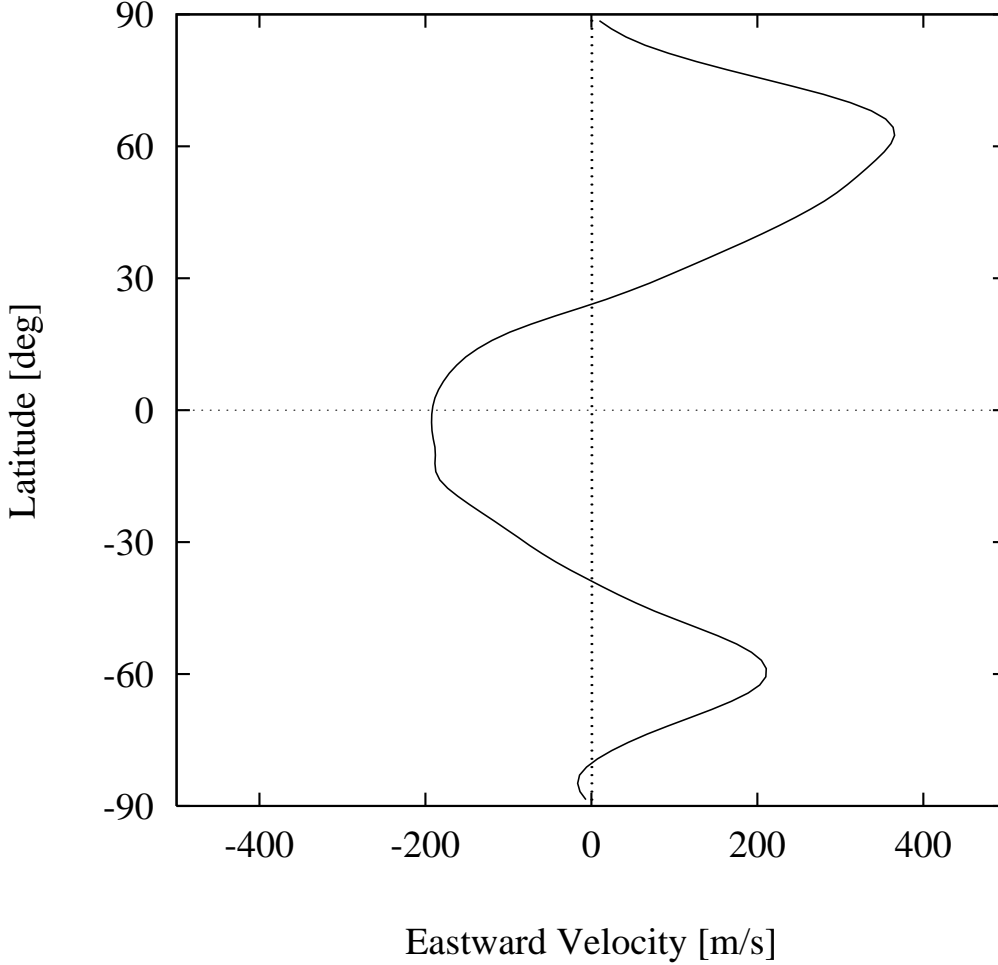


FIG. 2.— Steady circulation profile from the flow of Fig. 1: longitudinally-averaged zonal (eastward) wind velocity. Zonal jets emerge from a random initial condition due to conversion of small-scale stirring/eddies to planetary waves in the atmosphere (as seen in Fig. 1), a generic feature of shallow-layer turbulence under differential (latitudinally-dependent) rotation f . This basic profile has emerged approximately at day 20 of the simulation and does not change for the duration of the simulation (several hundred HD 209458 b days). On HD 209458 b, the jets are fewer, broader, and stronger than those observed on Jupiter. This is because HD 209458 b is hotter and rotating more slowly than Jupiter. Hemispheric thermal forcing is applied on this robust flow.

FIG. 3.— Four successive night-side views of the temperature field in orthographic projection (on HD 209458 b days indicated). A persistent “thermal dipole”, associated with the circumpolar vortices, revolves around the pole and provides high thermal contrasts that may be detectable in the planet’s observational signatures. In contrast to the simple, permanent day/night picture, the hottest atmospheric region is, at times, on the night side of the planet. These spots are long-lived, asymmetric (cold regions are more well-defined and have larger amplitude), and can serve as large areas of atmosphere with distinct chemistry and thermodynamics. The global equilibrium blackbody temperature of the atmosphere is taken to be 1400 K.

This figure "fig1.jpg" is available in "jpg" format from:

<http://arxiv.org/ps/astro-ph/0209227v2>

This figure "fig3.jpg" is available in "jpg" format from:

<http://arxiv.org/ps/astro-ph/0209227v2>